ACS OMEGA

http://pubs.acs.org/journal/acsodf

Article

Reaction Behavior and Influencing Mechanisms of Different Fly Ashes on the NO Removal by Using the Ultraviolet Irradiating Chlorite Method

Zili Zhang, Yao Lin,* Jianwei Meng,* Lei Wang, Qin Yao, Xiaohan Chen, Guodong Dai, Yi Zhao, and Runlong Hao*

Cite This: *ACS Omega* 2022, 7, 8739−8752

Read Online

ACCESS | Metrics & More | Article Recommendations | Supporting Information

ABSTRACT: Our previous work had demonstrated that UV/$NaClO_2$ was the best advanced oxidation method in terms of nitric oxide (NO) removal, but we have not studied the impact of the fly ash on NO removal under such conditions. For this, this paper selected six kinds of fly ashes and studied their effects on NO removal. The micromorphology, elemental composition, and the elemental oxidation states of these six fly ashes were characterized by scanning electron microscopy-energy-dispersive X-ray spectra, X-ray photoelectron spectroscopy, and inductively coupled plasma methods. The main inorganic components in the six fly ashes are metal oxides (Fe_2O_3/Fe_3O_4, SiO_2, Al_2O_3, ZnO, MgO, and TiO_2), carbonates (Na_2CO_3 and $CaCO_3$), and chlorides (NaCl, KCl, and $MgCl_2$). The experimental results suggested that high solubility was the premise condition for the fly ashes exhibiting an inhibitory effect on NO removal. Among all of the metal compounds, Fe_2O_3/Fe_3O_4 exhibited the highest inhibitory contribution rate to the NO removal (22.9−45.7%). The anions of Cl^- and CO_3^{2-} acted as scavengers for the free radicals which greatly impaired the oxidation of NO. Based on the simulation experimental results and the UV−vis analysis, the order of inhibitory contribution rates of various metal compounds to the NO removal was determined as $Fe_2O_3/Fe_3O_4 > TiO_2 \approx Na_2CO_3 > Al_2O_3 \approx ZnO \approx MnO_2 > CaCO_3 > NaCl > KCl \approx SiO_2 \approx MgCl_2$.

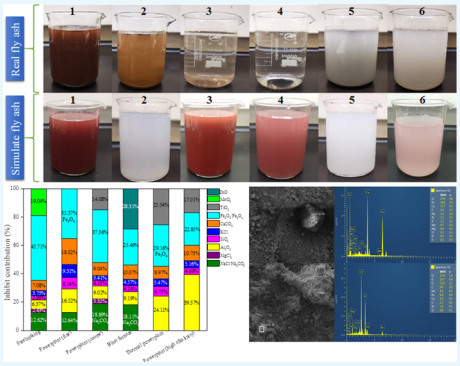

1. INTRODUCTION

Nitric oxide (NO) is a terrible air pollutant that can form acid rain, photochemical smog, and haze.[1] Stationary sources such as power plants and industrial boilers/furnaces[2,3] and mobile sources such as automobiles and ships are the main sources of NO emissions.[4,5] Selective non-catalytic reduction and selective catalytic reduction are mature flue gas denitrification technologies that have been widely applied in power plants and industrial boilers/furnaces, with ammonia and urea as the reductants.[6,7] As for the treatment of mobile source pollution, noble metal-induced three-way catalysis, such as Pd/Pt-based zeolite catalysts, is popularized in gasoline cars and diesel cars, with unburnt alkane and urea as the main reductants.[8,9] Intrinsically speaking, the aforementioned technologies belong to the harmless disposal of NO (NO → N_2), rather than the recycling method. As an important N-containing substance, converting NO to high value-added products such as nitrate-based compounds (ammonium nitrate or calcium ammonium nitrate) is more in accordance with the circular economy concept. Taking full use of the advanced oxidation process (AOP) is one of the good methods to realize this target.

Integrating AOP oxidation with wet absorption is considered to be a promising method for recovering NO.[10] The hydroxyl radical ($HO^•$), singlet oxygen ($^1O_2$), ozone (O_3), sulfate radicals ($SO_4^{•-}$), oxychloride radical ($ClO^•$), and chlorine dioxide (ClO_2) have been used to oxidize NO into nitrate. These radicals usually originated from common oxidants such as H_2O_2,[11] persulfate (PS),[12] oxone (PMS),[13] $NaClO_2$,[14] and NaClO,[15] and so on, and catalytic means including ultraviolet/vacuum ultraviolet (UV/VUV),[16] transition metals,[13,17,18] thermal,[12] microwave,[19] and sonic[20] have been used to yield these radicals. Compared with other catalysis methods, the UV- or VUV-induced AOP method is better from the view of practical application, which is due to the following advantages: (1) insensitive to the solution pH, (2) less energy consumption, (3) cost-efficient, and (4) less secondary environmental impact. UV-AOP methods mainly include UV/H_2O_2,[16] UV/PS and UV/PMS,[21,22] UV/NaClO,[23] and UV/$NaClO_2$,[14] and so forth.

In previous work,[24] we had demonstrated that UV/ClO_2^- showed an excellent performance in the removal of NO, with the

Received: December 7, 2021
Accepted: February 23, 2022
Published: March 3, 2022

https://doi.org/10.1021/acsomega.1c06930
ACS Omega 2022, 7, 8739−8752

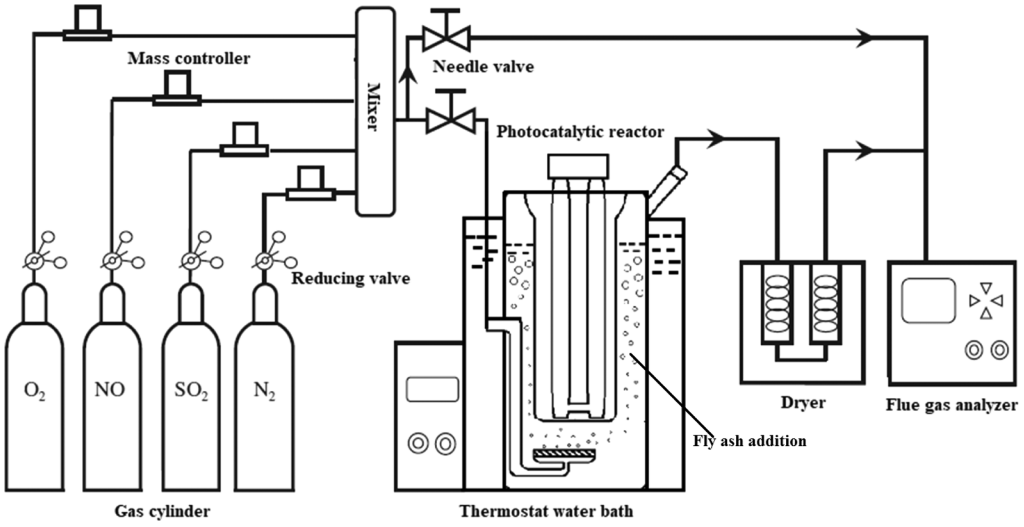

Figure 1. Experimental flow chart.

efficiency of 99.1%. Moreover, the ClO_2 generated from the photodecomposition of ClO_2^- (eqs 1 and 2) played a leading role in the NO removal process, but the yield of NO_2 was high since the yield of $ClO^•$ was low. To deal with this problem, NH_4OH was selected as an additive to suppress the formation of ClO_2, meanwhile increasing the $ClO^•$ yield (eq 3). Furthermore, we also systematically compared the performance and cost-effectiveness of the five typical UV-AOP methods (UV/H_2O_2, UV/PS, UV/PMS, UV/NaClO, and $UV/NaClO_2$) in the removal of NO and demonstrated that $NaClO_2$ possessed the highest absorbance at 254 nm (124.3 abs/mol), implying that it had the highest quantum yield. The experimental results indicated that $UV/NaClO_2$ was far superior to other UV−AOP methods in terms of the NO removal. The evolution of the radicals in the five UV−AOP systems under different pH and different SO_2 concentrations was unveiled. However, the reaction behavior of the fly ash during the NO removal process was not studied; thus, further exploring that the reaction behavior as well as its influencing mechanism in the NO removal is of great significance.

$$ClO_2^- + h\nu \rightarrow (ClO_2^-)^* \quad (1)$$

$$(ClO_2^-)^* + ClO_2^- \rightarrow ClO_2 + ClO^- + O^{\bullet -} \quad (2)$$

$$ClO_2^- + h\nu \rightarrow ClO^\bullet + O^{\bullet -} \quad (3)$$

As we all know, fly ash is a common component present in industrial flue gas, and it may affect the UV light penetration or quench the radicals to affect the oxidation process. However up to now, few studies have reported its influence on the UV-AOP method's ability to remove NO, especially the latest $UV/NaClO_2$. As well, the influencing mechanisms of different kinds of fly ashes on NO removal are also not clear now. Hence, the objective of this paper is to investigate the effects of different kinds of fly ashes on NO removal using the $UV/NaClO_2$ AOP method. The investigated fly ashes were sampled from some coal-fired power plants and steel mills. Based on the characterization analyses of different fly ashes and the experimental results on the NO removal in the presence of different fly ashes, the main inhibitors (metal oxides or non-metal oxides) in fly ashes were identified and their influencing mechanisms on the NO removal were revealed. The information provided in this paper may be of great significance for the application of $UV/NaClO_2$ in flue gas denitrification.

2. MATERIALS AND METHODS

2.1. Chemicals. All chemicals used in this study are of analytical grade. The $NaClO_2$ solution (0.5 mM) was prepared with $NaClO_2$ powders (80% wt) and deionized water. According to the characterization analysis results of different fly ashes, we used pure metal oxides, that is Fe_2O_3 (96.5% wt); Fe_3O_4 (99.0% wt); SiO_2 (99.0% wt); Al_2O_3 (99.0% wt); ZnO (99.0% wt); MgO (98.0% wt); TiO_2 (99.0%); carbonates, that is Na_2CO_3 (99.5% wt) and $CaCO_3$ (99.0% wt); and chlorides, that is NaCl (99.5% wt), KCl (99.5% wt), and $MgCl_2$ (99.0% wt) to simulate the components in fly ashes. These chemicals were purchased from the Aladdin Company. We used six kinds of fly ashes to conduct the NO removal experiments. They were sampled from the steelmaking factory, coal-fired power plant, blast furnace, and thermal power plant. Specifically, the first fly ash was sampled from a bag filter in some steelmaking factory. The second and third fly ashes are fine and coarse fly ashes, respectively, which were sampled from the fourth electric field and the first electric field of an electrostatic precipitator in some coal-fired power plant. The fourth fly ash was sampled from a bag filter in some blast furnace. The fifth fly ash was sampled from an electrostatic precipitator in some thermal power plant. The sixth fly ash is a kind of fly ash with high alkalinity, which was sampled from some coal-fired power plant in the northwest of China.

2.2. Experimental Apparatus. Figure 1 shows the experimental flow chart, which consists of simulated flue gas generation, a UV photolysis reactor, and tail gas detection. The core part is a cylinder and a jacketed quartz-wall UV-photolysis reactor, which is heated with a thermostat water bath. The diameter and height of the inner and outer cylinders are 60/96 mm and 140/200 mm, respectively. The low-pressure lamp (TUV PS-S, Philips Co., Beijing, 12 W, and the light intensities are 2.54×10^{-4} E·s^{-1}) is placed inside the cylinder. The temperature and pH of the composite solution are detected online using an inside thermocouple and a pH meter. During the experiments, the $NaClO_2$ solution will be first mixed with the fly ash and then be used to conduct the NO removal experiments. After drying the tail gas, the NO concentration of the inlet and

https://doi.org/10.1021/acsomega.1c06930
ACS Omega 2022, 7, 8739−8752

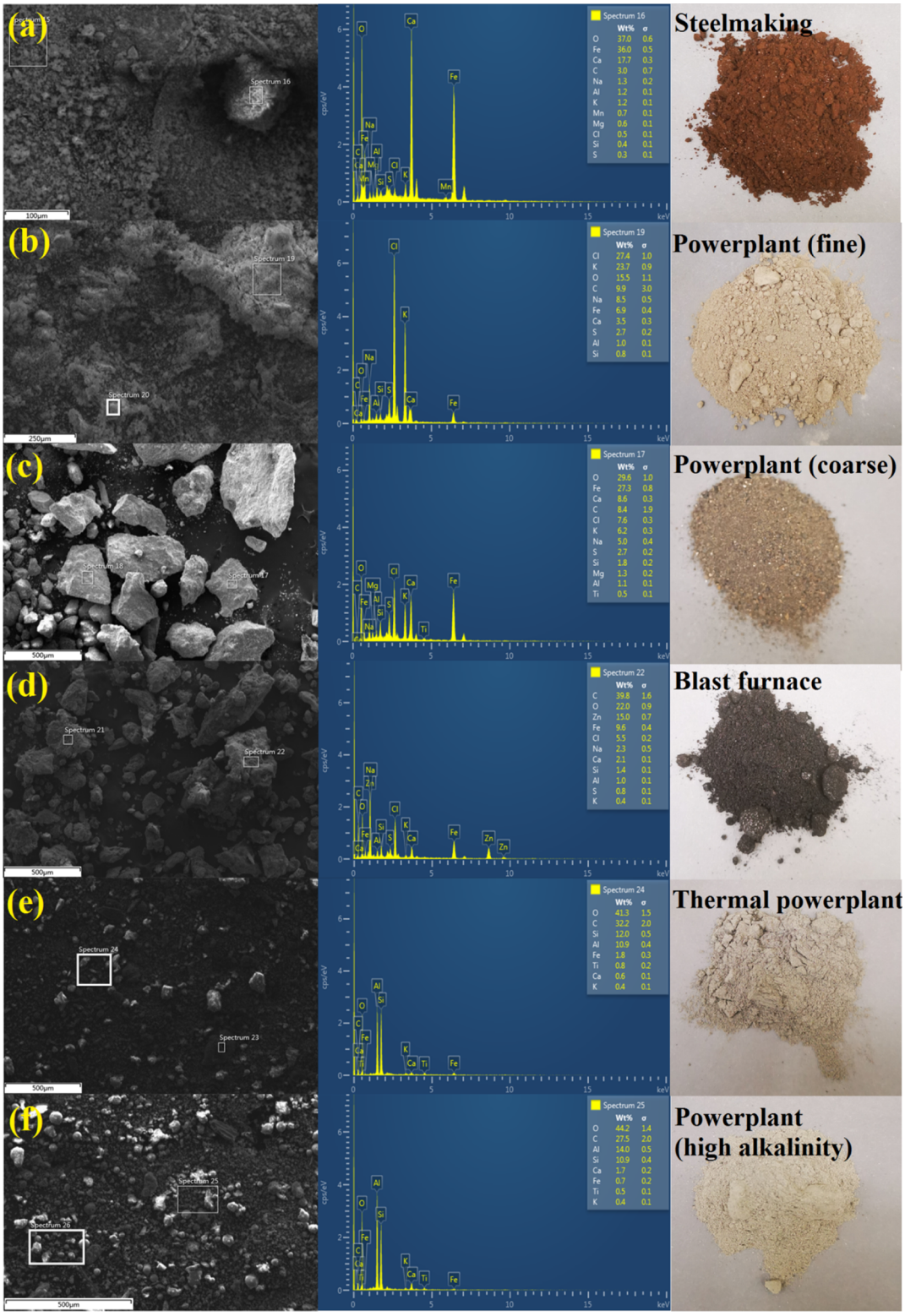

Figure 2. SEM−EDS analyses of the six fly ashes. (a) First fly ash; (b) second fly ash; (c) third fly ash; (d) fourth fly ash; (e) fifth fly ash; and (f) sixth fly ash.

outlet flue gases are detected by using an infrared flue gas analyzer (Photon, Madur Co, Austria). The efficiencies of NO conversion were calculated by eq 4.

$$\eta = \frac{(C_{in} - C_{out})}{C_{in}} \times 100\% \quad (4)$$

where η is the removal efficiency after an appropriate reaction time; C_{in} and C_{out} are the inlet and outlet concentrations of NO, mg/m^3, respectively.

2.3. Analytical Methods. Scanning electron microscopy (SEM) (Zeiss Ultra 60, Carl Zeiss NTS, LLC North America) was used for imaging the surface morphologies of different fly

https://doi.org/10.1021/acsomega.1c06930
ACS Omega 2022, 7, 8739−8752

ashes. The fly ashes were fixed on stubs with carbon dots and then sputter-coated with a 2 nm gold layer. Coated samples were examined under an accelerating voltage of 5 kV at different magnifications. Energy-dispersive X-ray spectra (EDS) of different fly ashes were also obtained using an energy dispersive spectroscopy analyzer (XF lash 5060FQ Annular EDX detector, Bruker, Germany). The binding energies of Na 1s, Mg 1s, Al 2p, K 2p, Ca 2p, Fe 2p, and Zn 2p in different fly ashes were analyzed by using X-ray photoelectron spectroscopy (XPS) (ESCA-LAB250 spectrometer with an Al Kα source (1486.6 eV)). The detection conditions are 10 kV voltage with a base pressure of 2×10^{-9} Mbar. The XPS characterization was conducted after drying and grinding the fly ashes. The contents of the metals in the six fly ashes were measured using an inductively coupled plasma source mass spectrometer (ICP−MS, 7700, Agilent Technology Co., USA).

3. RESULTS AND DISCUSSION

3.1. Fly Ashes Characterizations. Figure 2a−f show the SEM images and photographs of the six kinds of fly ashes. It can be found that the first and second fly ashes are presented in the form of adhesive superfine particles (<10 μm), and parts of them are agglomerated into blocks (the diameter ranges from tens to hundreds of microns). However, their colors are totally different: the first fly ash is reddish brown and the second fly ash is yellowish white. By contrast, the third and fourth fly ashes are presented in the form of incompact large particles (the diameter ranges from tens to hundreds of microns), and they look like stones with sharp edges and corners. It can be found in the photographs that the third fly ash is more like sand with a tan color, while the color of the fourth fly ash is black brown. Also, the fifth and sixth fly ashes are presented in the form of fine powders which are like flour and mainly consist of spheroidal particles. The color of the fifth fly ash is light gray and that of the sixth fly ash is pure white. According to the photographs, we could conclude that the fly ashes sampled from power plants were presented in light colors, while those sampled from steelmaking and blast furnaces were presented in deep colors. The results suggest that after thorough combustion, most of the combustible substances will be burned out by power plant boilers, and only a large number of inorganic salts will be remained; however, due to the high contents of metal oxides, the fly ashes sampled from steelmaking and the blast furnace will appear in the color of metal compounds.

Figure 2 also provides the EDS analysis results by which the elemental proportions are obtained, and the detailed data are available in Table S1. For the first fly ash, O and Fe are the main elements which account for 37.0% wt and 36.0% wt, respectively, suggesting that Fe is the most abundant metal in the first fly ash. The proportions of the other elements are 17.7% wt for Ca, 3.0% wt for C, 1.3% wt for Na, 0.6% wt for Mg, 1.2% wt for Al, 1.2% wt for K, and 0.7% wt for Mn, so the first fly ash possesses an abundant variety of metals. The blast furnace is also one of the steelmaking links, thus the fourth fly ash may also have abundant metals. However, it can be found in the fourth fly ash that the contents of Fe and O account for only 9.6 and 22.0% wt, respectively, while the contents of Zn and C are as high as 15.0 and 39.8%, respectively, so the fourth fly ash has a large amount of unburnt carbon and a high-value metal, Zn. The resource for the unburnt carbon mainly originated from the reductant coke. The second and third fly ashes are fine and coarse fly ashes sampled from the same coal-fired power plant. It can be found that compared with the coarse fly ash, the fine fly ash has more Cl, K, and Na but less O, Si, Ca, and Fe, so NaCl and KCl are easily enriched on fine particles, but Fe_2O_3, CaO, and SiO_2 are inclined to attaching onto the coarse fly ash. The fifth and sixth fly ashes are all sampled from the power plants in the northwest of China, and they are famous for their high alkalinity. The EDS analysis results of the fifth and sixth fly ashes verify this point: the contents of Al, Si, O, and C are as high as 10.9% wt/14.0wt, 12.0% wt/10.9% wt, 41.3% wt/44.2%, and 32.2% wt/27.5% wt, respectively. The results suggested that the alkaline Al_2O_3 and SiO_2 might suppress the coal's thorough combustion, resulting in a high content of unburnt carbon. One thing should be noted that the third, fifth, and sixth fly ashes also have little Ti, so these fly ashes may also contain TiO_2. In addition, the reddish brown color of the first fly ash and the black brown color of the fourth fly ash may be due to the presence of the high content of Fe and Zn, respectively.

As a result of the EDS analysis results, which can only give the elemental proportion of the fly ash surface, we further performed the ICP analysis to accurately unveil the metal constitution of the six kinds of fly ashes. Table 1 lists the ICP analysis results, including the metal content and metal proportion. The main metals in the first fly ash are Fe ≫ Ca ≫ Mg > Mn > K > Na > Al, in which the proportions of Fe and Ca are 46.43 and 6.76%, respectively. The main metals in the second fly ash are Fe > K > Zn > Ca > Na ≫ Mg > Al > Ti > Mn, in which the proportions of Fe, K, and Zn are 21.74, 12.62, and 6.57%, respectively. The main metals in the third fly ash are Fe ≫ Ca > K > Mg > Al > Ti > Na, in which the proportion of Fe is 34.15%. The main metals in the fourth fly ash are Fe ≫ Zn > Ca ≫ Al > Na > K, in which the proportions of Fe and Zn are 14.15 and 3.55%, respectively. The main metals in the fifth fly ash are Al > Fe > Ti > K > Ca, in which the proportions of Al and Fe are only 3.84 and 2.33%, respectively. The main metals in the sixth fly ash are Al > Fe > Ti > Ca > K, in which the proportions of Al and Fe are only 7.12 and 2.19%, respectively. From the view of elemental content, the Fe content in the first four fly ashes is hundreds of g per kg of fly ash, so Fe compounds should be the primary inorganic salt in the first four samples; also, the contents of Ca, K, Mg, Zn, and Na are high in different levels; the contents of Al and Fe in the last two fly ashes are tens of g per kg of fly ash. Thus, Al and Fe compounds should be the primary inorganic salt in the last two samples.

Furthermore, X-ray photoelectron spectroscopy was performed to determine the elemental oxidation states of the six fly ashes. All the data concerning the peak separation refer to the NIST X-ray Photoelectron Spectroscopy Database.[25] Figure 3 shows the spectra of Na 1s, Mg 1s, Al 2p, K 2p, Ca 2p, and Fe 2p of the first fly ash, in which the peak at 1071.0 eV is ascribed to NaCl or Na_2SO_4; the peaks at 1302.7 and 1303.9 eV are due to the presence of $Mg(OH)_2$ and MgO, respectively; the peak at 74.9 eV is assigned to Al_2O_3; the peaks at 292.7 and 295.2 eV are all assigned to KCl; the peaks at 346.5 and 350.3 eV are ascribed to CaO and $CaCO_3$, respectively; and the peaks at 710.9 and 724.0 eV are assigned to Fe_2O_3 and Fe_3O_4, respectively. Figures 4−8 represent the XPS spectra of the other five fly ashes, and Table S2 lists all the binding energies and the corresponding compounds. For the second fly ash, only Na 1s, Al 2p, K 2p, Ca 2p, and Fe 2p are detected. The peak at 1072.1 eV is attributed to NaCl or Na_2CO_3, the peaks at 74.6 and 77.3 eV are all ascribed to Al_2O_3, the peaks at 293.1 and 295.8 eV are all assigned to KCl, the peaks at 347.6 and 351.2 eV are ascribed to CaO and $CaCO_3$, respectively, and the peaks at 710.8 and 723.9 eV are attributed to Fe_2O_3 and Fe_3O_4, respectively. The

https://doi.org/10.1021/acsomega.1c06930
ACS Omega 2022, 7, 8739−8752

Table 1. ICP Analysis Results of the Six fly Ashes

sample	element	elemental content (mg/kg)	elemental proportion (%)
the first fly ash	Fe	464312.9	46.43
	Ca	67636.9	6.76
	Mg	13306.8	1.33
	Mn	9001.1	0.90
	K	8469.3	0.85
	Na	7768.3	0.78
	Al	2613.8	0.26
the second fly ash	Fe	217434.3	21.74
	K	126217.2	12.62
	Zn	65720.2	6.57
	Ca	45294.4	4.53
	Na	32200.1	3.22
	Mg	7201.2	0.72
	Al	4949.5	0.49
	Ti	3082.0	0.31
	Mn	763.1	0.08
the third fly ash	Fe	341506.5	34.15
	Ca	52074.7	5.21
	K	11016.8	1.10
	Mg	10532.4	1.05
	Al	7140.4	0.71
	Ti	6463.5	0.65
	Na	4212.5	0.42
the fourth fly ash	Fe	141503.6	14.15
	Zn	35530.3	3.55
	Ca	23149.6	2.31
	Al	8569.2	0.86
	Na	2268.0	0.23
	K	1636.8	0.16
the fifth fly ash	Al	38443.2	3.84
	Fe	23257.4	2.33
	Ti	5436.6	0.54
	K	4380.4	0.44
	Ca	3512.7	0.35
the sixth fly ash	Al	71199.4	7.12
	Fe	21944.5	2.19
	Ti	6951.1	0.70
	Ca	5551.2	0.56
	K	1182.3	0.12

constitution of the third fly ash is the same as that of the second fly ash, namely NaCl/Na_2CO_3, Al_2O_3, KCl, CaO/$CaCO_3$, and Fe_2O_3/Fe_3O_4 because they are generated under the same combustion conditions. As for the fourth fly ash, the XPS spectra of Na 1s, Al 2p, K 2p, Ca 2p, Fe 2p, and Zn 2p were observed, and the peak separation process is the same as mentioned above. A new peak at 1022.5 eV corresponding to Zn 2p is assigned to the formation of ZnO. Hence, the constitution of the fourth fly ash is NaCl/Na_2CO_3, Al_2O_3, KCl, CaO/$CaCO_3$, Fe_2O_3/Fe_3O_4, and ZnO. The fifth and sixth samples are highly alkaline fly ashes, and only the XPS spectra of Al 2p, Ca 2p, and Fe 2p are detected. The fifth fly ash possesses the metal compounds of Al_2O_3, CaO/$CaCO_3$, and Fe_2O_3/Fe_3O_4, and the sixth fly ash has the metal compounds of Al_2O_3, $CaCO_3$, and Fe_2O_3.

3.2. Effects of Fly Ashes and the Corresponding Inorganic Salts on the NO Removal. Based on the above ICP and XPS analysis results, we can carry out the following investigating experiments more effectively. Then, we studied the effects of the six fly ashes on the NO removal by using UV/$NaClO_2$. As shown in Figure 9A, without fly ash, the NO removal efficiency obtained by using UV/$NaClO_2$ alone is 85.6%. After adding the six fly ashes, the NO removal efficiency is sharply decreased from 85.6 to 45, 33, 66, 60, 52, and 66%, respectively, which demonstrates that fly ash is a powerful inhibitor which can greatly suppress the radical-induced oxidation of NO. Furthermore, the inhibition order is 2 > 1 > 5 > 4 > 3 = 6. The inhibitory effect of the fly ashes may be due to the following reasons: (1) the inorganic salts in the fly ash may quench the radical species such as $^{\bullet}OH$, $ClO^{\bullet}$, and Cl_2O_2,[26−28] resulting in the decrease in the radical yield and radical activity, so the oxidation efficiency of NO is declined; (2) on the other hand, adding fly ash will make the solution turbid and further impact UV light penetrating, so as a result, the ClO_2^- molecules are difficult to effectively absorb the UV_{254} photons, resulting in the decrease in the oxidation ability of the reaction system. In order to verify the above speculation and find out which factor is the main reason causing the decrease in NO removal efficiency, the following experiments were carried out.

In previous studies, it had been demonstrated that the free radicals could react with the chloride ions and the carbonate ions to form various secondary free radicals, such as $ClOH^{\bullet-}$, $Cl_2^{\bullet-}$, and $CO_3^{\bullet-}$.[26,27,29,30] According to the EDS and XPS analysis results, the six fly ashes have chloride and carbonate, so we first studied their effects on the NO removal using NaCl, $MgCl_2$, and KCl as the chemicals to simulate the chlorides. As shown in Figure 9B, when NaCl is used as the chloride and with the Cl concentration rising from 1.1 to 7.4 mM, a slight decrease in the NO removal efficiency from 85.6 to 82.5% appears. When NaCl is substituted with $MgCl_2$, the NO removal efficiency is constant at around 85%. If KCl is used and the concentration is adjusted from 0.2 to 12.2 mM, the NO removal efficiency is stable in the range of 82−85%. Hence, from the aforementioned experimental results, chlorides exhibited a slight inhibitory effect on UV/$NaClO_2$ removing NO, and the excess chloride did not significantly suppress the NO removal process. According to the studies,[29,30] although Cl^- could quench radicals such as $HO^{\bullet}$ to decline the oxidation capacity of the reaction system, it could also produce a number of secondary free radicals such as $Cl^{\bullet}$ and $ClOH^{\bullet-}$ (eqs 5 and 6), and the in situ-produced $Cl^{\bullet}$ and $ClOH^{\bullet-}$ were reported to be capable of being useful for the removal of NO. Hence, adding chloride will not significantly affect the NO removal process.

$$^{\bullet}OH + Cl^- \rightarrow OH^- + Cl^{\bullet} \quad (5)$$

$$OH + Cl^- \rightarrow ClOH^{\bullet-} \quad (6)$$

$$HO^{\bullet} + HCO_3^- \rightarrow CO_3^{\bullet-} + H_2O \quad (7)$$

Figure 9C shows the impact of the carbonate on UV/$NaClO_2$ in removing NO. When we used Na_2CO_3 as the carbonate and increased the CO_3^{2-} concentration to 0.6−3.7 mM, the NO removal efficiency decreased from 85.6 to 73.3−74.7%; but if we used $CaCO_3$ as the carbonate and increased its concentration to 0.9−8.9 mM, the NO removal efficiency just decreased from 85.6 to 79.5−82.1%. It could be found that both of the two carbonates had an inhibitory effect on UV/$NaClO_2$ in removing NO, but the inhibition resulting from Na_2CO_3 was larger than that of $CaCO_3$. The difference in the inhibitory effect is mainly due to the difference in the solubility of the two carbonates: Na_2CO_3 is freely soluble while $CaCO_3$ is slightly soluble. According to the previous studies,[26,27] CO_3^{2-} could quench $HO^{\bullet}$ to form the secondary radical $CO_3^{\bullet-}$ (eq 7), but the

https://doi.org/10.1021/acsomega.1c06930
ACS Omega 2022, 7, 8739−8752

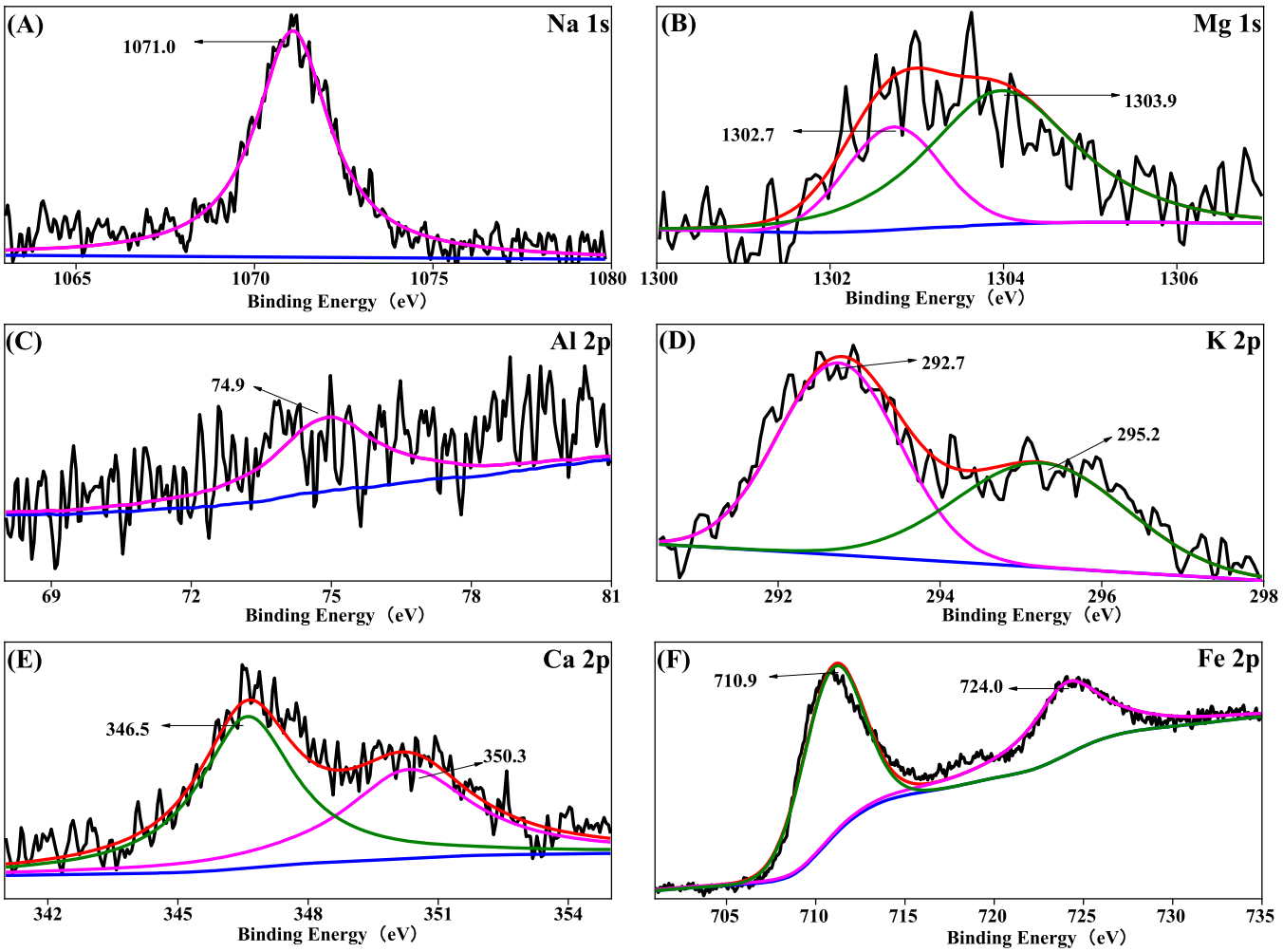

Figure 3. XPS analysis of the fly ash sampled from a steelmaking factory (the first fly ash). Na 1s (A); Mg 1s (B); Al 2p (C); K 2p (D); Ca 2p (E); and Fe 2p (F).

oxidation capacity of $CO_3^{\bullet-}$ is weaker than that of $HO^{\bullet}$, so the NO removal efficiency was decreased in the presence of carbonate. We could also find that the variation in the carbonate content would not greatly impact the NO removal process, implying that CO_3^{2-} only affected the yield of $HO^{\bullet}$ and not the yield of Cl radicals. Moreover, Cl radicals such as ClO_2, $ClO^{\bullet}$, and Cl_2O_2 contributed more to the NO removal, which had been demonstrated by the previous studies.[14] Thus, the NO removal efficiency was not significantly changed with the variation in carbonate concentrations.

Furthermore, we studied the effect of the aluminum salt and silicon salt on the NO removal. According to the XPS analysis results, Al_2O_3 and SiO_2 are the main existing forms of Al and Si in the fly ashes, so we used Al_2O_3 and SiO_2 as the chemicals to study their effects on NO removal. As shown in Figure 9D, as the Al_2O_3 concentration increases to 0.4−5.0 mM, the removal efficiency of NO significantly decreases from 85.6 to 63−81%. Thus, Al_2O_3 was demonstrated to be a strong radical inhibitor for the UV/$NaClO_2$ denitrification system. As for the effect of SiO_2, it can be found that the NO removal process will be unaffected by SiO_2, and the removal efficiency of NO is constant at 85%, so SiO_2 is harmless for the radical-induced oxidation of NO. As we all know, the light transmittance of Al_2O_3 is less than that of SiO_2; thus, the light propagation in Al_2O_3 is more difficult than that of SiO_2. Hence, due to the decrease in the UV luminous flux, the radical yield would be greatly decreased after Al_2O_3 addition. As a result, the NO removal process was suppressed.

According to the EDS, XPS, and ICP analysis results, Fe is the most abundant metal in the six fly ashes and the main existing forms of Fe are Fe_2O_3 and Fe_3O_4. Therefore, the effects of Fe_2O_3 and Fe_3O_4 on the removal of NO were further studied. As shown in Figure 9E, when the concentrations of Fe_2O_3 and Fe_3O_4 increase to 0.13−6.4 and 0.08−4.3 mM, respectively, the NO removal efficiency significantly decreases to 41.5−79.5 and 53.0−73.3%, respectively. Consequently, the inhibitory impacts of Fe_2O_3 and Fe_3O_4 would be intensified with the increase in Fe contents, and their inhibitory impacts are comparable. Fe_2O_3 and Fe_3O_4 have deep colors, which can reduce the luminous flux of UV light, and the photon utilization rate would be decreased and the oxidation of NO would be inhibited. Besides, Fe_3O_4 and Fe_2O_3 would be decomposed into Fe^{2+} under UV light irradiation (eq 8),[18,20] and the produced Fe^{2+} would then consume $OH^{\bullet}$ (eq 9), ClO_2, $ClO^{\bullet}$, and Cl_2O_2, causing the decline of the NO removal efficiency.

$$Fe_3O_4 + h\nu \rightarrow Fe^{2+} + 2e^- \quad (8)$$

$$Fe^{2+} + OH^{\bullet} \rightarrow Fe^{3+} + OH^- \quad (9)$$

https://doi.org/10.1021/acsomega.1c06930
ACS Omega 2022, 7, 8739−8752

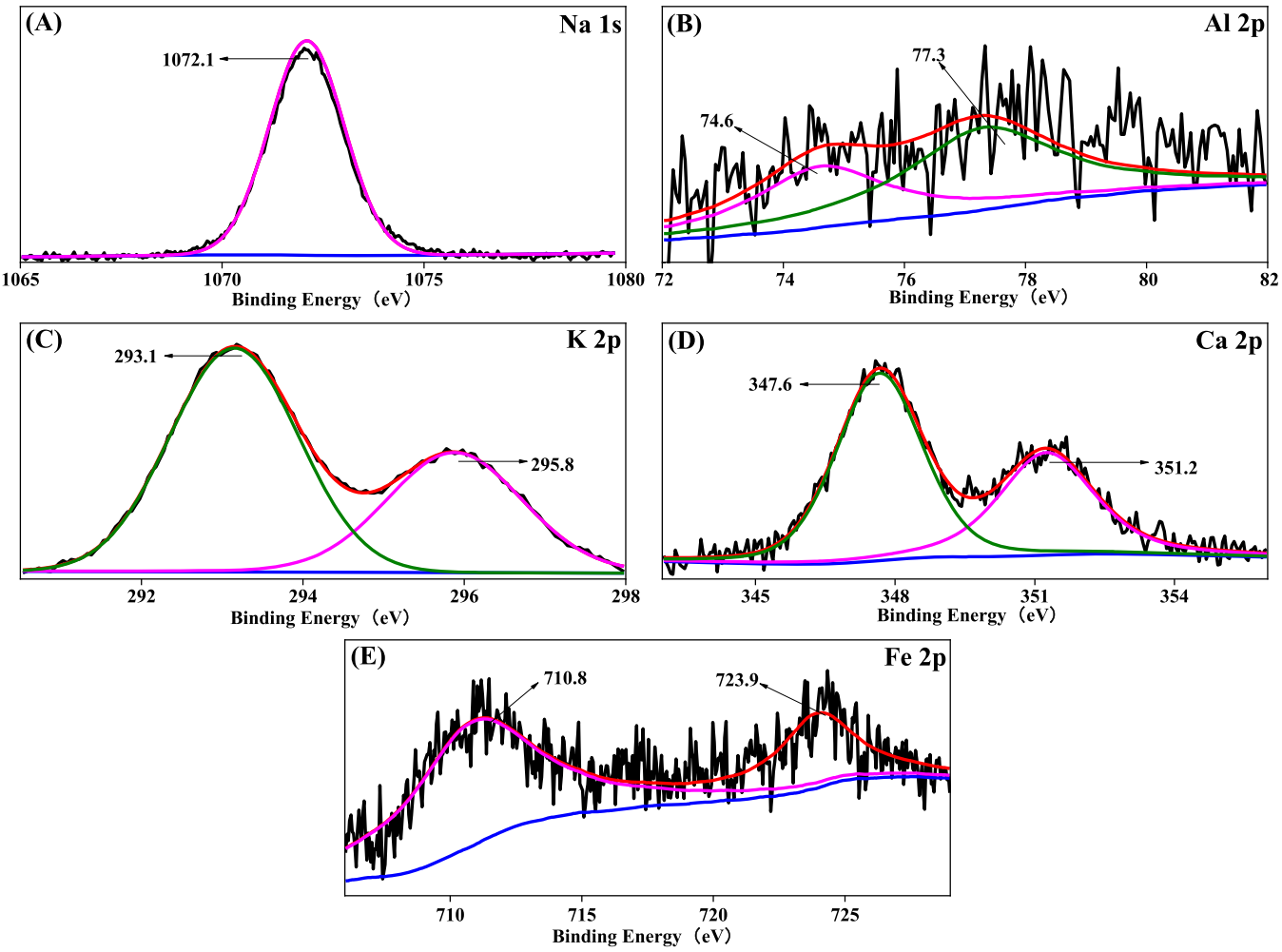

Figure 4. XPS analysis of the fine fly ash sampled from some coal-fired power plant (the second fly ash). Na 1s (A); Al 2p (B); K 2p (C); Ca 2p (D); and Fe 2p (E).

The contents of Ti, Mn, and Zn in fly ash are relatively small, but they may also affect NO removal, so we studied the effects of TiO_2, MnO_2, and ZnO on the NO removal. As shown in Figure 9F, when 0.3 mM TiO_2, 0.3 mM MnO_2, and 4.6 mM ZnO are used, the NO removal efficiencies decrease to 72, 68, and 67%, respectively. TiO_2, MnO_2, and ZnO have strong shielding effects in UV light, so they can reduce the luminous flux, resulting in the decrease in radical yield and inhibiting the oxidation of NO. Besides, the addition of fly ash will also increase the turbidity of the solution. In addition, the turbidity will hinder the passage of light in the solution. Thus, we investigated the turbidity on the NO removal, and the results are shown in Figure S1. It can be seen that when the turbidity rises from 1 to 900, the removal efficiency of NO is almost unchanged, suggesting that the turbidity of the solution is not the main inhibitory factor for the radical-induced oxidation of NO.

3.3. Mechanism Analysis. In order to reveal the influencing mechanism of the aforementioned fly ashes as well as their metal oxides on the removal of NO, we used pure metal compounds including Fe_2O_3/Fe_3O_4, $NaCl/Na_2CO_3$, $CaO/CaCO_3$, KCl, SiO_2, Al_2O_3, $MgCl_2$, TiO_2, ZnO, and MnO_2 to simulate the fly ash slurries to conduct the NO removal experiments. Figure 10A provides comparable photographs of the real and simulated fly ash solutions. It can be found that the first, the fifth, and the sixth simulated fly ash solutions are presented in a similar form and color to those of the real ones; the third and the fourth simulated fly ash solutions are different from the real ones, which is mainly due to the fact that the third and the fourth real fly ashes are more like stones (as illuminated in SEM images). Thus, they cannot be evenly dispersed in the solution without violent agitation. On the other hand, the simulated samples are totally prepared with pure chemicals, while the real ones definitely contain lots of impurities, so the simulated fly ash solution is more transparent and brighter, therefore they cannot be totally the same in color.

Accordingly, we performed comparing experiments on NO removal in the presence of the simulated and real fly ashes. The corresponding experimental results are shown in Figure 10B. It can be found that the NO removal efficiencies obtained in the presence of simulated fly ashes are close to those obtained in the presence of real fly ash, and the differences in the NO removal efficiencies are only 3.74, 27.12, 10.65, 2.81, 1.07, and 3.15%, respectively. In consideration of the allowable error bars, the inhibitory effect caused by the simulated fly ashes can be considered basically consistent with the real ones. Therefore, the harmful impact resulting from the six fly ashes on the NO removal is mainly due to the synergistic function of different types of metal or non-metal compounds.

In order to determine the inhibitory contribution rates of different metal compounds to the NO removal, we got the

https://doi.org/10.1021/acsomega.1c06930
ACS Omega 2022, 7, 8739−8752

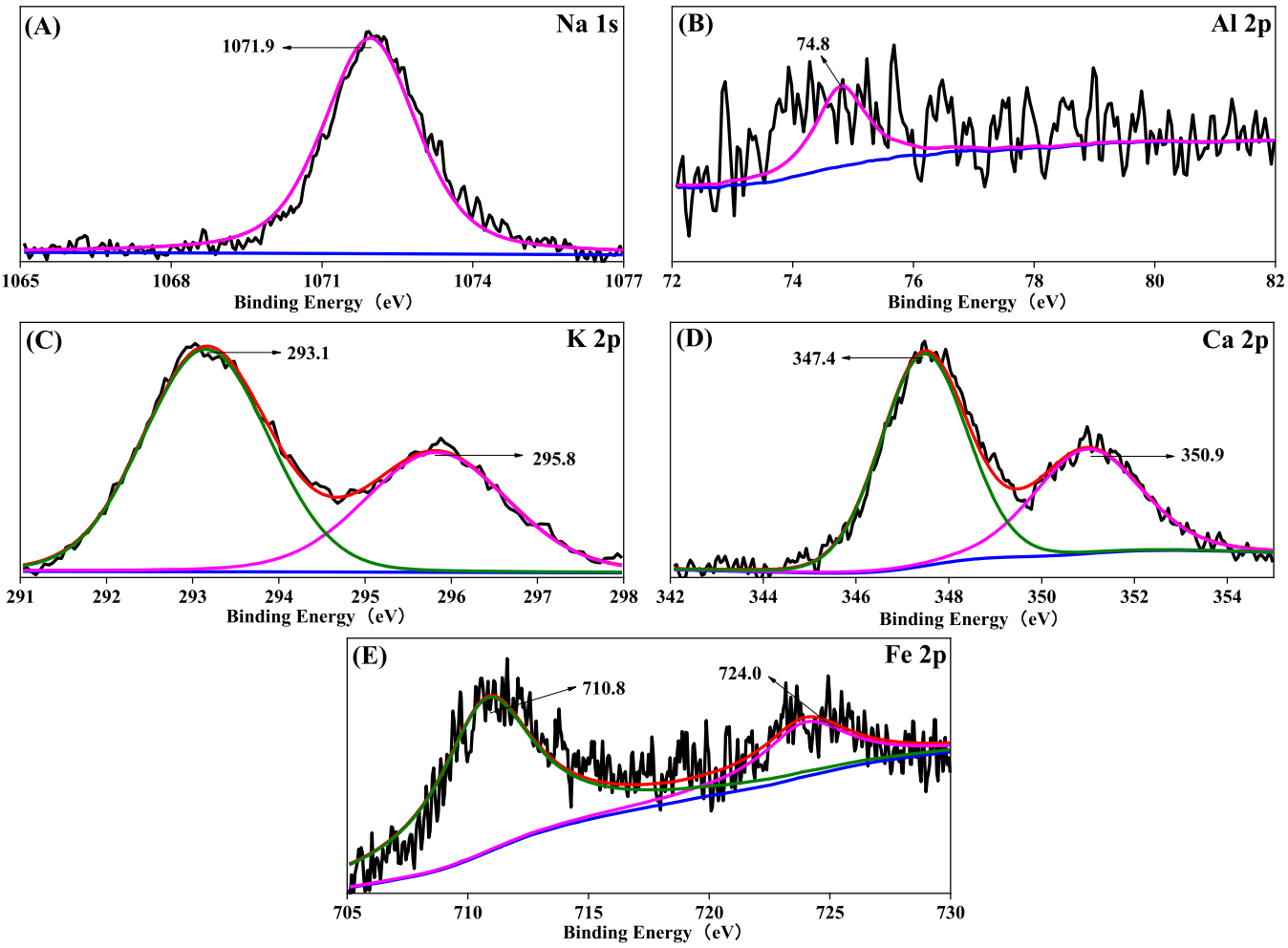

Figure 5. XPS analysis of the coarse fly ash sampled from some coal-fired power plant (the third fly ash). Na 1s (A); Al 2p (B); K 2p (C); Ca 2p (D); and Fe 2p (E).

suppression sum of the different metal oxides and, respectively, calculated their inhibitory contribution rates to the NO removal. As shown in Figure 10C, for the first fly ash, the order of the inhibitory contribution rate on the NO removal is Fe_2O_3/Fe_3O_4 (45.7%) > MnO_2 (19.0%) > $NaCl/Na_2CO_3$ (12.6%) > $CaCO_3$ (7.1%) > Al_2O_3 (6.4%) > KCl (3.8%) ≈ SiO_2 (3.0%) ≈ $MgCl_2$ (2.4%). For the second fly ash, the order of the inhibitory contribution rate is Fe_2O_3/Fe_3O_4 (35.4%) > $CaCO_3$ (18.0%) > Al_2O_3 (16.5%) > $NaCl/Na_2CO_3$ (12.6%) > KCl (9.3%) ≈ SiO_2 (8.1%). For the third fly ash, the order of the inhibitory contribution rate is Fe_2O_3/Fe_3O_4 (37.4%) > $NaCl/Na_2CO_3$ (18.9%) > TiO_2 (14.1%) > $CaCO_3$ (9.0%) = Al_2O_3 (9.0%) > SiO_2 (4.2%) > KCl (3.4%) ≈ $MgCl_2$ (3.3%). For the fourth fly ash, the order of the inhibitory contribution rate is ZnO (28.3%) > Fe_2O_3/Fe_3O_4 (25.5%) > $NaCl/Na_2CO_3$ (18.1%) > $CaCO_3$ (10.1%) > Al_2O_3 (9.2%) > KCl (4.6%) ≈ SiO_2 (4.2%). For the fifth fly ash, the order of the inhibitory contribution rate is Fe_2O_3/Fe_3O_4 (29.2%) > TiO_2 (25.5%) > Al_2O_3 (24.1%) > $CaCO_3$ (9.0%) > SiO_2 (6.8%) ≈ KCl (5.5%). For the sixth fly ash, the order of the inhibitory contribution rate is Al_2O_3 (39.6%) > Fe_2O_3/Fe_3O_4 (22.9%) > TiO_2 (17.0%) > $CaCO_3$ (10.7%) > KCl (5.2%) ≈ SiO_2 (4.7%). It can be found that the inhibitory contribution rate of Fe_2O_3/Fe_3O_4 is the highest among all of the metal compounds. Additionally, the inhibitory contribution rates of $NaCl/Na_2CO_3$, Al_2O_3, TiO_2, ZnO, and MnO_2 are relatively high in consideration of their contents in the fly ashes. Specifically, the content of Ti in fly ash is much smaller than that of Zn, inferring that the inhibitory effect of Ti is stronger than Zn under equal content. The inhibitory contribution rate of Al is affected by its content in fly ash. If the contents of Al and Zn are close in fly ash, their inhibitory effects are very close, which indicates that their inhibitory effect on the NO removal is comparable. The inhibitory contribution rates of MnO_2, $CaCO_3$, and $NaCl/Na_2CO_3$ are also very close. However, the content of Mn in fly ash is much smaller than that of Ca and Na. Therefore, the inhibitory effect of MnO_2 is higher than that of $CaCO_3$ and $NaCl/Na_2CO_3$. As illuminated by the ICP results, the content of Ca in fly ash is much higher than that of Na; thus, the inhibitory contribution rate of Na_2CO_3 is significantly higher than that of $CaCO_3$. Combining with the experimental results in Figure 9B,C, it can be found that the inhibitory effect of NaCl is far less than that of $NaCO_3$. Hence, the order of the inhibitory contribution rate to the NO removal of $CaCO_3$, NaCl, and Na_2CO_3 is Na_2CO_3>$CaCO_3$>NaCl. As for the inhibitory effects of KCl, $MgCl_2$, and SiO_2, their inhibitory contribution rates are similar and will not be significantly changed with their content variation. Finally, according to the above analyses combined with the EDS, XPS, and ICP characterization analyses and the experimental results, the order of the overall inhibitory contribution rates of all of the metal compounds to the NO removal can be concluded as

https://doi.org/10.1021/acsomega.1c06930
ACS Omega 2022, 7, 8739−8752

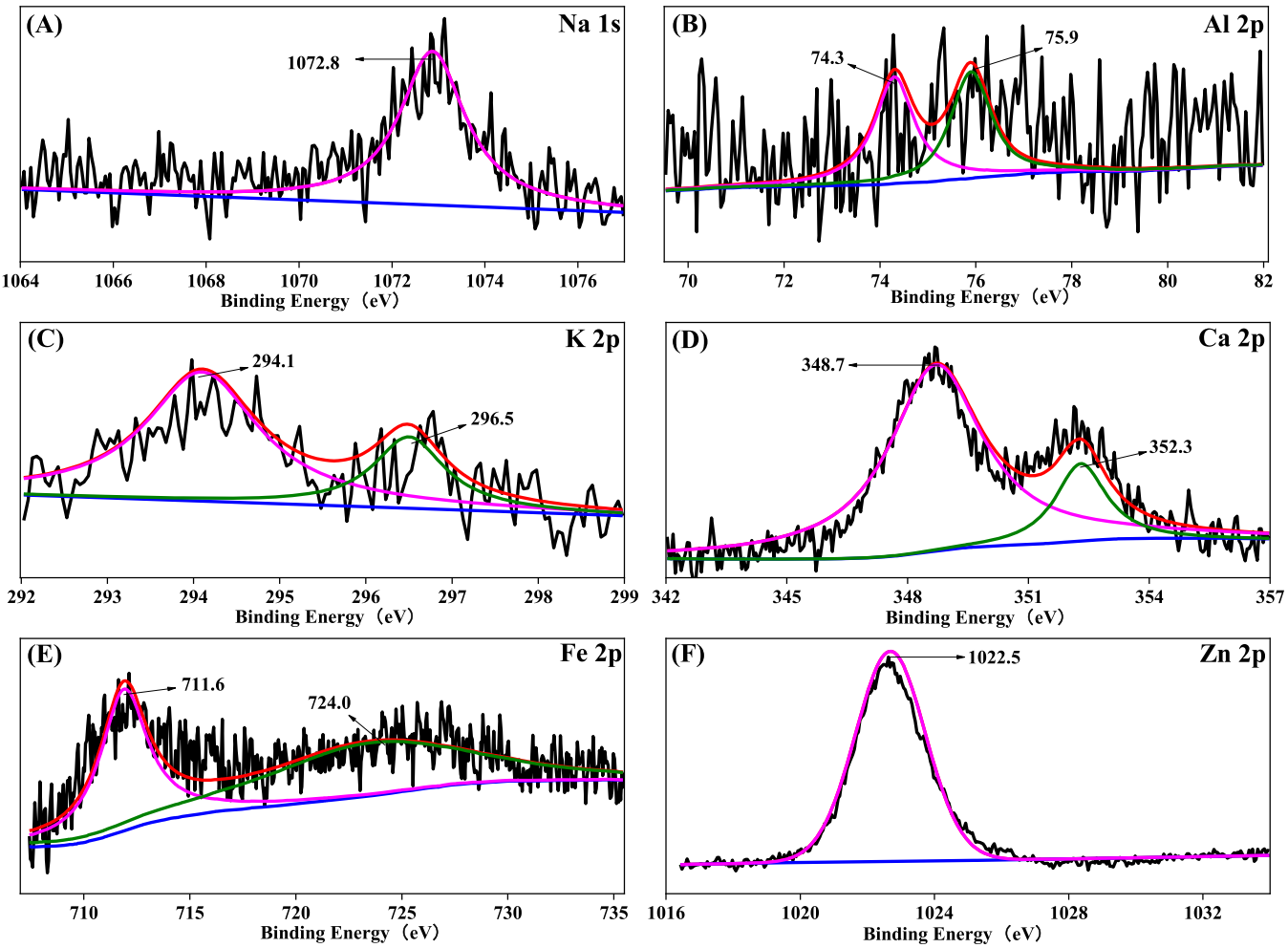

Figure 6. XPS analysis of the fly ash sampled from some blast furnace (the fourth fly ash). Na 1s (A); Al 2p (B); K 2p (C); Ca 2p (D); Fe 2p (E); and Zn 2p (F).

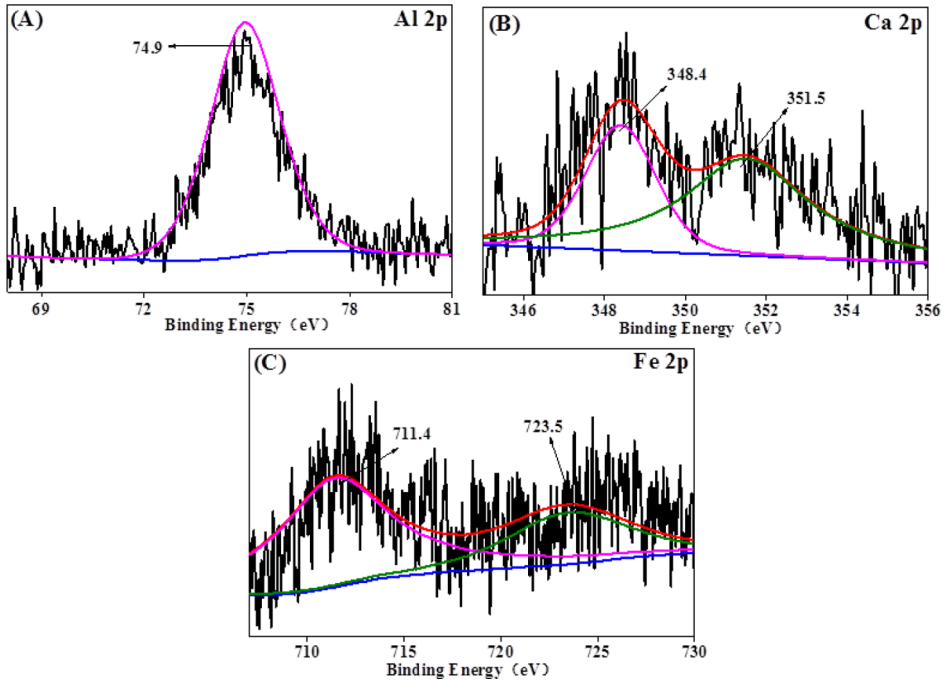

Figure 7. XPS analysis of the fly ash sampled from some thermal power plant (the fifth fly ash). Al 2p (A); Ca 2p (B); and Fe 2p (C).

https://doi.org/10.1021/acsomega.1c06930
ACS Omega 2022, 7, 8739−8752

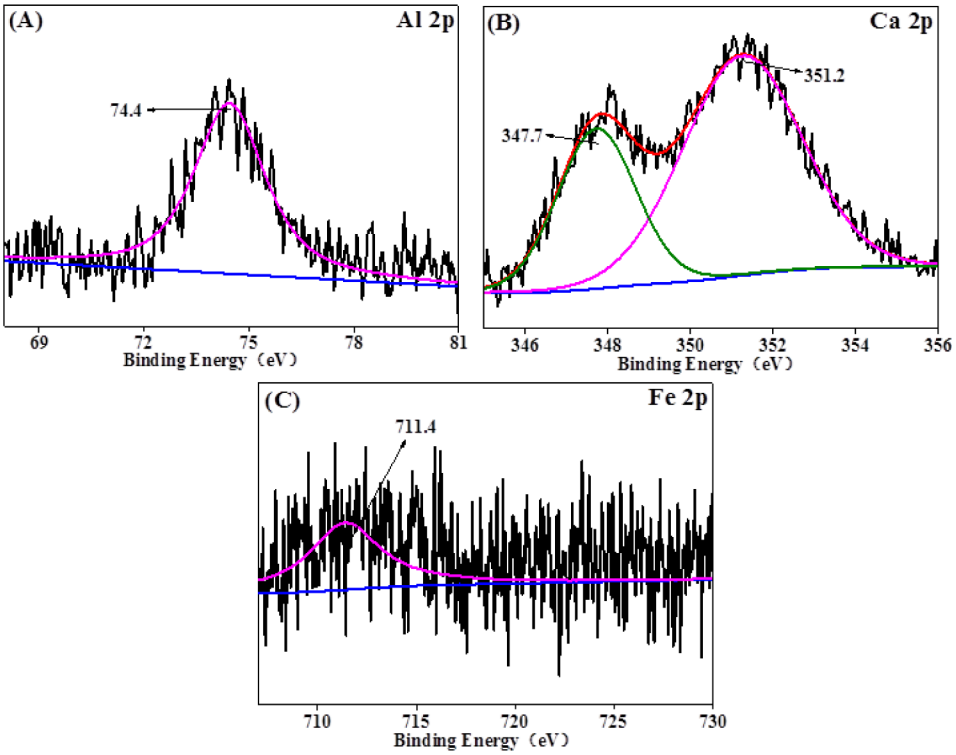

Figure 8. XPS analysis of the high alkaline fly ash sampled from some coal-fired power plant (the sixth fly ash). Al 2p (A); Ca 2p (B); and Fe 2p (C).

follows: Fe_2O_3/Fe_3O_4 > TiO_2 ≈ Na_2CO_3 > Al_2O_3 ≈ ZnO ≈ MnO_2 > $CaCO_3$ > NaCl > KCl ≈ SiO_2 ≈ $MgCl_2$.

How do these metal compounds affect the radical-induced oxidation of NO? We need to illuminate this issue. As mentioned in Section 3.2, anions such as Cl^- and CO_3^{2-} can quench the free radicals to form various secondary free radicals such as $ClOH^{\bullet-}$, $Cl_2^{\bullet-}$, and $CO_3^{\bullet-}$ and then further impair the oxidation capacity of the UV/$NaClO_2$ system. The other metal compounds may not be capable to rapidly scavenge the free radicals, but they can impact the UV light penetration and absorb the high-energy photons to suppress the radical formation. Therefore, we further tested the absorbance of the six fly ashes as well as their metal oxides under UV_{254} light, and the results are shown in Figure 10D,E. It can be found that adding the first, second, fifth, and sixth fly ashes can greatly increase the absorbance of the $NaClO_2$ solution, suggesting that these four fly ashes can effectively absorb the UV_{254} light. However, it can also be found that adding the third and fourth fly ashes does not increase the absorbance, which is mainly because their particle sizes are so big and they cannot be dissolved in the solution, as demonstrated in Figure 10A. By contrast, the turbidities of the first, second, fifth, and sixth fly ashes are higher, indicating that the metal compounds in these four fly ashes were solved or at least suspended in the solution. Hence, the relatively high solubility is the premise condition to compare the inhibitory contributions of different fly ashes to NO removal. We further studied the UV_{254} light absorbance of different metal oxides and anions at equivalent levels to compare their shading effects on the UV_{254} light. As shown in Figure 10E, their light shading effects in a descending order are TiO_2 (799.9 Abs/mol) > MnO_2 (558.5 Abs/mol) > Fe_3O_4 (398.8 Abs/mol) > Fe_2O_3 (358.1 Abs/mol) > CO_3^{2-} (232.8 Abs/mol) > SiO_2 (144.5 Abs/mol) > Al_2O_3 (131.9 Abs/mol) > ZnO (106.2 Abs/mol) ≈ Cl^- (78.2 Abs/mol). Hence, TiO_2, MnO_2, Fe_3O_4, Fe_2O_3, and CO_3^{2-} could greatly suppress the UV light utilization and decrease the radical yield.

Based on the aforementioned analyses, it can be concluded that if the fly ashes can be highly dissolved in the solution, the following metal oxides will greatly affect the UV light utilization. (1) Because of the high content, Fe_2O_3/Fe_3O_4 will act as the primary inhibitor for the radical formation; (2) soluble anions such as Cl^- and CO_3^{2-} will change the solution constitution to change the radical species to decline the oxidation capacity of the reaction system; and (3) during the aforementioned process, TiO_2, MnO_2, SiO_2, Al_2O_3, and ZnO with low contents will also participate in the inhibitory reaction to affect the radical-induced oxidation of NO from two aspects: one is the absorption of high-energy photons, and the other is inducing radical quenching or making the free radicals inactive.

4. CONCLUSIONS

In this paper, the influencing mechanisms of six typical fly ashes on the NO removal by using UV/$NaClO_2$ were studied. The micromorphology, elemental composition, and the elemental oxidation states of the six fly ashes were revealed. The inhibitory effect of the six fly ashes on the NO removal was illuminated by changing the composition and content of different metal compounds. The mechanism analysis suggested that high solubility is the premise condition for the fly ashes exhibiting an inhibitory effect on the NO removal. Fe_2O_3/Fe_3O_4 exhibited the highest inhibitory contribution rate to NO removal. The anions of Cl^- and CO_3^{2-} acted as scavengers to quench the free radicals and impair the oxidation capacity of the UV/$NaClO_2$ system. The order of the overall inhibitory contribution rate of metal compounds in fly ash on the NO removal was determined as Fe_2O_3/Fe_3O_4 > TiO_2 ≈ Na_2CO_3 > Al_2O_3 ≈ ZnO ≈ MnO_2 > $CaCO_3$ > NaCl > KCl ≈ SiO_2 ≈ $MgCl_2$.

https://doi.org/10.1021/acsomega.1c06930
ACS Omega 2022, 7, 8739−8752

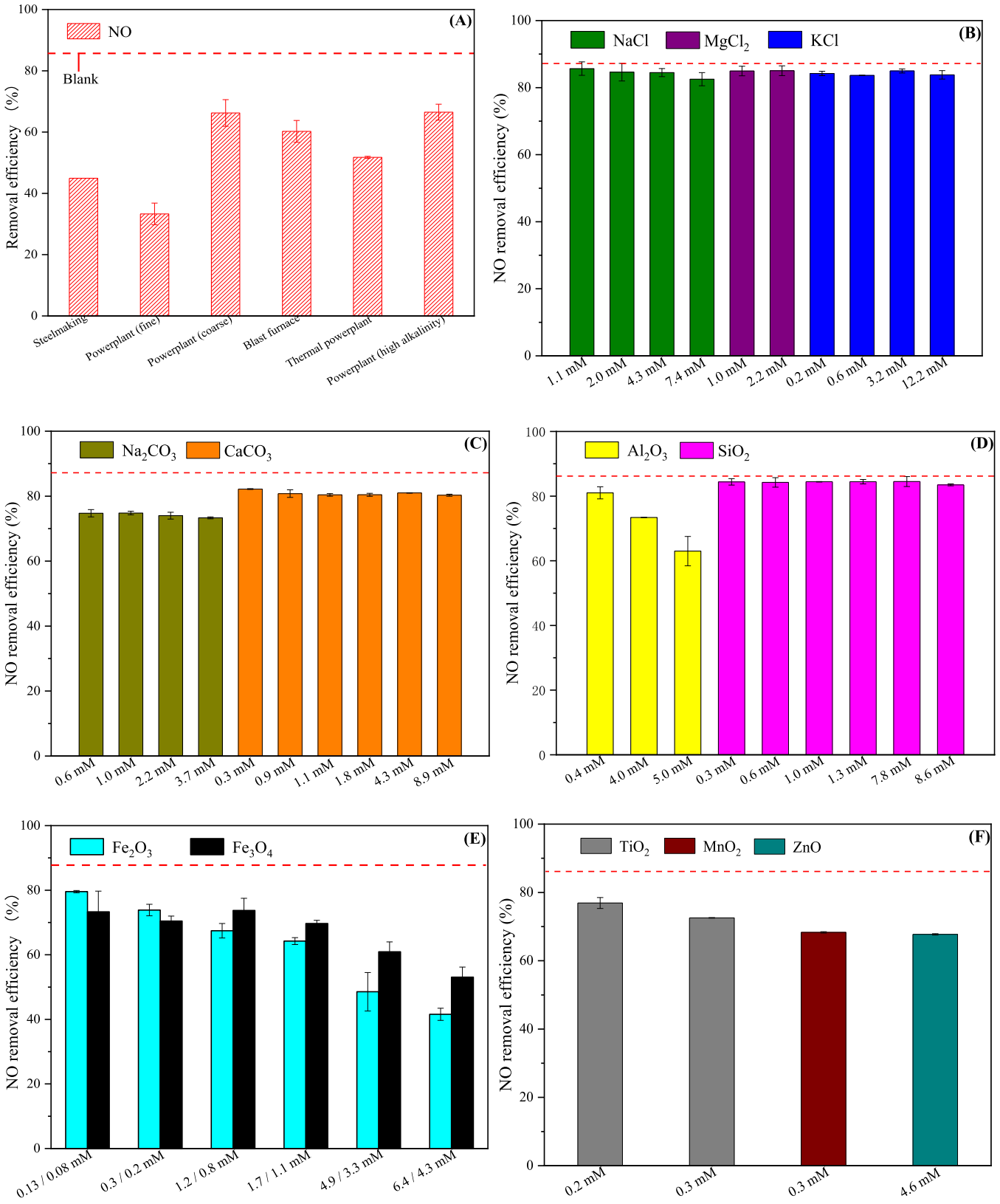

Figure 9. Effect of the six fly ashes on the NO removal using the UV/$NaClO_2$ method (A); effect of chloride on the NO removal (B); effect of carbonate on the NO removal (C); effects of Al_2O_3 and SiO_2 on the NO removal (D); effects of Fe_2O_3 and Fe_3O_4 on the NO removal (E); and effects of TiO_2, MnO_2, and ZnO on the NO removal (F). The $NaClO_2$ concentration is 5 mM, the UV_{254} light power is 14 W, the volume of reaction solution is 500 mL, and the reaction temperature is 50 °C.

https://doi.org/10.1021/acsomega.1c06930
ACS Omega 2022, 7, 8739−8752

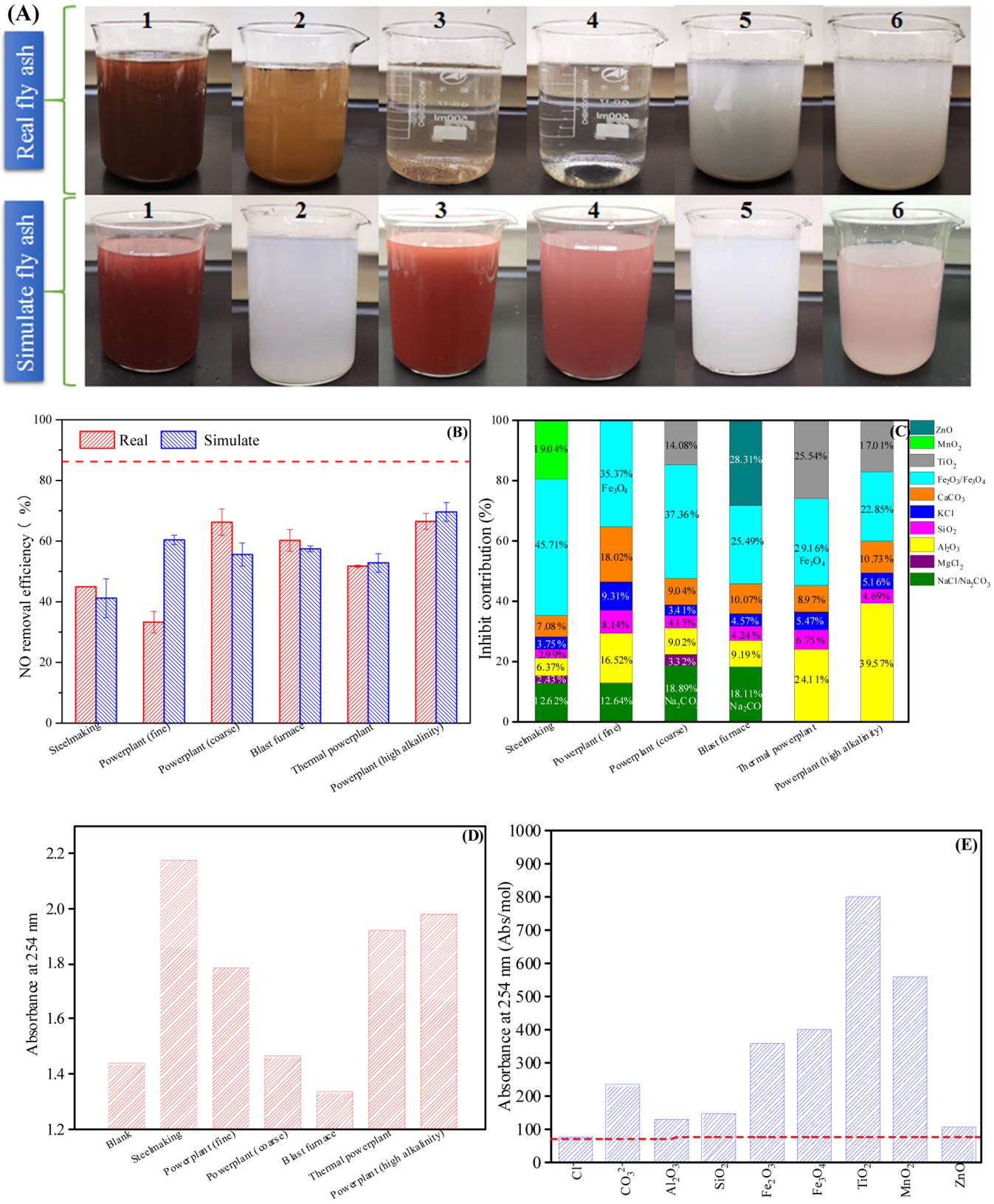

Figure 10. Comparable photographs of the real fly ash and simulated fly ash solutions (A); effect of the real and simulated fly ashes on the NO removal (B); inhibitory contribution rates of different metal compounds to the NO removal (C); absorbance of the six fly ashes under UV_{254} light (D); absorbance of different metal oxides and anions under UV_{254} light (E). The $NaClO_2$ concentration is 5 mM, the UV_{254} light power is 14 W, the volume of reaction solution is 500 mL, and the reaction temperature is 50 °C.

https://doi.org/10.1021/acsomega.1c06930
ACS Omega 2022, 7, 8739−8752

■ ASSOCIATED CONTENT

Supporting Information

The Supporting Information is available free of charge at https://pubs.acs.org/doi/10.1021/acsomega.1c06930.

Effect of turbidity on NO removal, EDS analysis results of the six fly ashes, and XPS analysis results of the six fly ashes (PDF)

■ AUTHOR INFORMATION

Corresponding Authors

Yao Lin − *Fujian Special Equipment Inspection and Research Institute, Fujian Boiler & Pressure Vessel Inspection and Research Institute, National Industrial Boiler Quality Inspection Center (Fujian), Fuzhou 350008, PR China*; Email: 417770734@qq.com

Jianwei Meng − *Hebei Key Laboratory of Mineral Resources and Ecological Environment Monitoring, Baoding 071000, PR China*; Email: mjw678@sina.com

Runlong Hao − *Hebei Key Lab of Power Plant Flue Gas Multi-Pollutants Control, Department of Environmental Science and Engineering, North China Electric Power University, Baoding 071003, PR China*; orcid.org/0000-0002-2793-3607; Email: hrl_ncepu@hotmail.com

Authors

Zili Zhang − *Fujian Special Equipment Inspection and Research Institute, Fujian Boiler & Pressure Vessel Inspection and Research Institute, National Industrial Boiler Quality Inspection Center (Fujian), Fuzhou 350008, PR China*

Lei Wang − *Hebei Key Laboratory of Mineral Resources and Ecological Environment Monitoring, Baoding 071000, PR China*

Qin Yao − *Fujian Special Equipment Inspection and Research Institute, Fujian Boiler & Pressure Vessel Inspection and Research Institute, National Industrial Boiler Quality Inspection Center (Fujian), Fuzhou 350008, PR China*

Xiaohan Chen − *Fujian Special Equipment Inspection and Research Institute, Fujian Boiler & Pressure Vessel Inspection and Research Institute, National Industrial Boiler Quality Inspection Center (Fujian), Fuzhou 350008, PR China*

Guodong Dai − *Fujian Special Equipment Inspection and Research Institute, Fujian Boiler & Pressure Vessel Inspection and Research Institute, National Industrial Boiler Quality Inspection Center (Fujian), Fuzhou 350008, PR China*

Yi Zhao − *Hebei Key Lab of Power Plant Flue Gas Multi-Pollutants Control, Department of Environmental Science and Engineering, North China Electric Power University, Baoding 071003, PR China*; orcid.org/0000-0001-9974-0348

Complete contact information is available at: https://pubs.acs.org/10.1021/acsomega.1c06930

Notes

The authors declare no competing financial interest.

■ ACKNOWLEDGMENTS

The authors appreciate the financial support provided by the National Natural Science Foundation of China (no. 52170108, no. 51978262, and no. 52000067), the Natural Science Foundation of Hebei Province (no. E2021502002 and no. E2020502033), the Local Science and Technology Development Guided by the Central Government (2019L3020), the State Administration for Market Regulation (2019MK035), the Fujian Provincial Department of Science and Technology (2020Y0055), and the Hebei Key Laboratory of Mineral Resources and Ecological Environment Monitoring (no. HBMREEM202102).

■ REFERENCES

(1) Liu, Y.; Shan, Y.; Wang, Y. Novel Simultaneous Removal Technology of NO and SO_2 Using a Semi-Dry Microwave Activation Persulfate System. *Environ. Sci. Technol.* **2020**, *54*, 2031−2042.

(2) Tong, Y.; Gao, J.; Wang, K.; Jing, H.; Wang, C.; Zhang, X.; Liu, J.; Yue, T.; Wang, X.; Xing, Y. Highly-Resolved Spatial-Temporal Variations of Air Pollutants from Chinese Industrial Boilers. *Environ. Pollut.* **2021**, *289*, 117931.

(3) Zhang, S.; Jiang, X.; Lv, G.; Wu, L.; Li, W.; Wang, Y.; Fang, C.; Jin, Y.; Yan, J. Co-Combustion of Shenmu Coal and Pickling Sludge in a Pilot Scale Drop-Tube Furnace: Pollutants Emissions in Flue Gas and Fly Ash. *Fuel Process. Technol.* **2019**, *184*, 57−64.

(4) Yang, S.; Han, Z.; Pan, X.; Liu, B.; Zhao, D. Nitrogen Oxide Removal from Simulated Flue Gas by UV-Irradiated Electrolyzed Seawater: Efficiency Optimization and pH-Dependent Mechanisms. *Chem. Eng. J.* **2018**, *354*, 653−662.

(5) Huo, Y.; Liu, K.; Liu, J.; He, H. Effects of SO_2 on Standard and Fast SCR over $CeWO_x$: A Quantitative Study of the Reaction Pathway and Active Sites. *Appl. Catal., B* **2022**, *301*, 120784.

(6) Lv, Y.; Wang, Z.; Zhou, J.; Cen, K. Full-Scale Numerical Investigation of a Selective Noncatalytic Reduction (SNCR) System in a 100 MW Utility Boiler with Complex Chemistry and Decoupling Approach. *Energy Fuels* **2010**, *24*, 5432−5440.

(7) Lai, J.-K.; Wachs, I. E. A Perspective on the Selective Catalytic Reduction (SCR) of NO with NH_3 by Supported V_2O_5−WO_3/TiO_2 Catalysts. *ACS Catal.* **2018**, *8*, 6537−6551.

(8) Zhan, Z.; Song, L.; Liu, X.; Jiao, J.; Li, J.; He, H. Effects of Synthesis Methods on the Performance of Pt + Rh/$Ce_{0.6}Zr_{0.4}O_2$ Three-Way Catalysts. *J. Environ. Sci.* **2014**, *26*, 683−693.

(9) Zhan, Z.; Liu, X.; He, H.; Song, L.; Li, J.; Ma, D. Fabrication of a Flower-Like Pd/CeO_2 Material with Improved Three-Way Catalytic Performance. *J. Rare Earths* **2013**, *31*, 750−758.

(10) Yuan, B.; Mao, X.; Wang, Z.; Hao, R.; Zhao, Y. Radical-Induced Oxidation Removal of Multi-Air-Pollutant: A Critical Review. *J. Hazard. Mater.* **2020**, *383*, 121162.

(11) Liu, Y.; Wang, Y.; Wang, Q.; Pan, J.; Zhang, Y.; Zhou, J.; Zhang, J. A Study on Removal of Elemental Mercury in Flue Gas Using Fenton Solution. *J. Hazard. Mater.* **2015**, *292*, 164−172.

(12) Liu, Y.; Wang, Q. Removal of Elemental Mercury from Flue Gas by Thermally Activated Ammonium Persulfate in A Bubble Column Reactor. *Environ. Sci. Technol.* **2014**, *48*, 12181−12189.

(13) Liu, Y.; Wang, Y. Elemental Mercury Removal from Flue Gas Using Heat and Co^{2+}/Fe^{2+} Coactivated Oxone Oxidation System. *Chem. Eng. J.* **2018**, *348*, 464−475.

(14) Hao, R.; Mao, X.; Qian, Z.; Zhao, Y.; Wang, L.; Yuan, B.; Wang, K.; Liu, Z.; Qi, M.; Crittenden, J. Simultaneous Removal of SO_2 and NO Using a Novel Method of Ultraviolet Irradiating Chlorite−Ammonia Complex. *Environ. Sci. Technol.* **2019**, *53*, 9014−9023.

(15) Liu, Y.; Wang, Y.; Liu, Z.; Wang, Q. Oxidation Removal of Nitric Oxide from Flue Gas Using UV Photolysis of Aqueous Hypochlorite. *Environ. Sci. Technol.* **2017**, *51*, 11950−11959.

(16) Liu, Y.; Wang, Q.; Pan, J. Novel Process of Simultaneous Removal of Nitric Oxide and Sulfur Dioxide Using a Vacuum Ultraviolet (VUV)-Activated O_2/H_2O/H_2O_2 System in A Wet VUV−Spraying Reactor. *Environ. Sci. Technol.* **2016**, *50*, 12966−12975.

(17) Yang, S.; Xu, D.; He, S.; Yan, W.; Xiong, Y. Modified Fe-Rich Palygorskite as an Efficient and Low-Cost Heterogeneous Fenton Catalyst for NO_x and SO_2 Removal. *Energy Fuels* **2020**, *34*, 8493−8502.

(18) Huang, Y.; Liang, Y.; Rao, Y.; Zhu, D.; Cao, J.-j.; Shen, Z.; Ho, W.; Lee, S. C. Environment-Friendly Carbon Quantum Dots/$ZnFe_2O_4$ Photocatalysts: Characterization, Biocompatibility, and Mechanisms for NO Removal. *Environ. Sci. Technol.* **2017**, *51*, 2924−2933.

(19) Hao, R.; Wang, Z.; Gong, Y.; Ma, Z.; Qian, Z.; Luo, Y.; Yuan, B.; Zhao, Y. Photocatalytic Removal of NO and Hg^0 Using Microwave Induced Ultraviolet Irradiating H_2O/O_2 Mixture. *J. Hazard. Mater.* **2020**, *383*, 121135.
(20) Liu, Y.; Liu, Z.; Wang, Y.; Yin, Y.; Pan, J.; Zhang, J.; Wang, Q. Simultaneous Absorption of SO_2 and NO from Flue Gas Using Ultrasound/Fe^{2+}/Heat Coactivated Persulfate System. *J. Hazard. Mater.* **2018**, *342*, 326−334.
(21) Cai, L.; Li, L.; Yu, S.; Guo, J.; Kuppers, S.; Dong, L. Formation of Odorous by-Products During Chlorination of Major Amino Acids in East Taihu Lake: Impacts of UV, UV/PS and UV/H_2O_2 Pre-Treatments. *Water Res.* **2019**, *162*, 427−436.
(22) Xie, R.; Ji, J.; Guo, K.; Lei, D.; Fan, Q.; Leung, D. Y. C.; Huang, H. Wet Scrubber Coupled with UV/PMS Process for Efficient Removal of Gaseous VOCs: Roles of Sulfate and Hydroxyl Radicals. *Chem. Eng. J.* **2019**, *356*, 632−640.
(23) Zhang, B.; Wang, X.; Fang, Z.; Wang, S.; Shan, C.; Wei, S.; Pan, B. Unravelling Molecular Transformation of Dissolved Effluent Organic Matter in UV/H_2O_2, UV/Persulfate, and UV/Chlorine Processes Based on FT-ICR-MS Analysis. *Water Res.* **2021**, *199*, 117158.
(24) Hao, R.; Ma, Z.; Qian, Z.; Gong, Y.; Wang, Z.; Luo, Y.; Yuan, B.; Zhao, Y. New Insight into the Behavior and Cost-Effectiveness of Different Radicals in the Removal of NO and Hg^0. *Chem. Eng. J.* **2020**, *385*, 123885.
(25) Naumkin, A. V.; Vass, A. K.; Gaarenstroom, S. W.; Powell, C. J. *NIST Standard Reference Database 20*, 2012, Version 4.1.
(26) Guo, K.; Wu, Z.; Shang, C.; Yao, B.; Hou, S.; Yang, X.; Song, W.; Fang, J. Radical Chemistry and Structural Relationships of PPCP Degradation by UV/Chlorine Treatment in Simulated Drinking Water. *Environ. Sci. Technol.* **2017**, *51*, 10431−10439.
(27) Kong, X.; Wu, Z.; Ren, Z.; Guo, K.; Hou, S.; Hua, Z.; Li, X.; Fang, J. Degradation of Lipid Regulators by the UV/Chlorine Process: Radical Mechanisms, Chlorine Oxide Radical (ClO•)-Mediated Transformation Pathways and Toxicity Changes. *Water Res.* **2018**, *137*, 242−250.
(28) Lyon, B. A.; Dotson, A. D.; Linden, K. G.; Weinberg, H. S. The Effect of Inorganic Precursors on Disinfection Byproduct Formation During UV-Chlorine/Chloramine Drinking Water Treatment. *Water Res.* **2012**, *46*, 4653−4664.
(29) Adewuyi, Y. G.; Owusu, S. O. Ultrasound-Induced Aqueous Removal of Nitric Oxide from Flue Gases: Effects of Sulfur Dioxide, Chloride, and Chemical Oxidant. *J. Phys. Chem. A* **2006**, *110*, 11098−11107.
(30) Fang, J.; Zhao, Q.; Fan, C.; Shang, C.; Fu, Y.; Zhang, X. Bromate Formation from the Oxidation of Bromide in the UV/Chlorine Process with Low Pressure and Medium Pressure UV Lamps. *Chemosphere* **2017**, *183*, 582−588.

https://doi.org/10.1021/acsomega.1c06930
ACS Omega 2022, 7, 8739−8752